Modular structure of functional networks in olfactory memory

David Meunier, Pierre Fonlupt, Anne-Lise Saive, Jane Plailly, Nadine Ravel, Jean-Pierre Royet

Modular structure of functional networks in olfactory memory

David Meunier [a*], Pierre Fonlupt [b], Anne-Lise Saive [a], Jane Plailly [a], Nadine Ravel [a],

Jean-Pierre Royet [a**]

[a] Olfaction: from coding to memory team, INSERM U1028, CNRS UMR 5292 – Université Lyon 1, Lyon F-69366, France.
[b] Brain, Dynamics and Cognition team, INSERM U1028, CNRS UMR 5292 – Université Lyon 1, Bron F-69675, France.

Abbreviated Title: Functional networks in olfactory memory

*** Corresponding Author:** **David Meunier**

Olfaction: from coding to memory team,

INSERM U1028, CNRS UMR 5292
50, Avenue Tony Garnier
Université Lyon 1, Lyon F-69366, France,
Phone: +33 (0)4 37 28 74 96
Fax: +33 (0)4 37 28 76 01
David.Meunier@olfac.univ-lyon1.fr

**** Corresponding Author:** **Jean-Pierre Royet**

Olfaction: from coding to memory team,

INSERM U1028, CNRS UMR 5292
50, Avenue Tony Garnier
Université Lyon 1, Lyon F-69366, France,
Phone: +33 (0)4 37 28 74 95
Fax: +33 (0)4 37 28 76 01
royet@olfac.univ-lyon1.fr

Abstract

Graph theory enables the study of systems by describing those systems as a set of nodes and edges. Graph theory has been widely applied to characterize the overall structure of data sets in the social, technological, and biological sciences, including neuroscience. Modular structure decomposition enables the definition of sub-networks whose components are gathered in the same module and work together closely, while working weakly with components from other modules. This processing is of interest for studying memory, a cognitive process that is widely distributed. We propose a new method to identify modular structure in task-related functional magnetic resonance imaging (fMRI) networks. The modular structure was obtained directly from correlation coefficients and thus retained information about both signs and weights. The method was applied to functional data acquired during a yes-no odor recognition memory task performed by young and elderly adults. Four response categories were explored: correct (Hit) and incorrect (False alarm, FA) recognition and correct and incorrect rejection. We extracted time series data for 36 areas as a function of response categories and age groups and calculated condition-based weighted correlation matrices. Overall, condition-based modular partitions were more homogeneous in young than elderly subjects. Using partition similarity-based statistics and *a posteriori* statistical analyses, we demonstrated that several areas, including the hippocampus, caudate nucleus, and anterior cingulate gyrus, belonged to the same module more frequently during Hit than during all other conditions. Modularity values were negatively correlated with memory scores in the Hit condition and positively correlated with bias scores (liberal/conservative attitude) in the Hit and FA conditions. We further demonstrated that the proportion of positive and negative links between areas of different modules (i.e., the proportion of correlated and anti-correlated areas) accounted for most of the observed differences in signed modularity. Taken together, our results provided some evidence that the neural networks involved in odor recognition memory are organized into modules and that these modular partitions are linked to behavioral performance and individual strategies.

Keywords

Graph theory, Functional connectivity, Neural network, Modularity, Olfactory memory, Signal detection theory

Introduction

Most cerebral imaging functional studies have used univariate statistical analyses to localize brain regions involved in specific cognitive operations (Rissman et al., 2004). However, the concept of the brain as a large complex network of interconnected elements has become dominant in modern neuroscience (Mesulam, 1990; Varela et al., 2001). Understanding how brain regions specifically communicate with one another during a particular cognitive task remains challenging.

The term "brain connectivity" is used at the functional level to describe the organization, interrelationships, and integrated performance of different brain regions (Horwitz, 2003). A distinction is made between methods that consider correlation or covariance between signals in different regions (functional connectivity) and methods that attempt to describe or make inferences about the direction of influence between regions (effective connectivity) (Friston, 1994; Rogers et al., 2007). Techniques for measuring functional connectivity during tasks include correlations between standardized regression coefficients (Rissman et al., 2004), principal and independent component analysis (PCA and ICA) (McKeown and Sejnowski, 1998; Calhoun et al., 2001), and graph theoretical methods (Bullmore and Sporns, 2009; Fornito et al., 2013). Techniques that measure effective connectivity include psychophysiological interaction (PPI) (Friston et al., 1997), structural equation modeling (SEM) (Mclntosh and Gonzalez-Lima, 1994), Granger causal mapping (Roebroeck et al., 2011), and dynamic causal modeling (DCM) (Friston et al., 2003; Penny et al., 2004).

While several studies have explored the functional connectivity of the olfactory network in animals (e.g., Wilson and Yan, 2010; Wilson et al., 2011; Spors et al., 2012), very few human cerebral imaging studies have been performed, and most have used effective connectivity. Zald et al. (1998) used covariance matrices based on PET data to elucidate the functional connectivity between the amygdala and the orbitofrontal cortex (OFC) during emotional olfactory tasks. Plailly et al. (2008) combined functional magnetic resonance imaging (fMRI) with DCM to measure attention-dependent network coherence within olfactory pathways. Haase et al. (2011) used SEM to

test a functional connectivity model during recognition memory in individuals genetically at risk for Alzheimer's disease. Karunanayaka et al. (2013) used whole-brain ICA decomposition to identify subcomponents involved in olfactory perception as well as SEM to study the directionality of interactions between these subcomponents. PPI analyses have also been used to demonstrate amplified functional connectivity between several olfactory-related regions, either in response to negative odors, particularly in anxiety (Krusemark and Li, 2012), or during passive smelling (Nigri et al., 2013).

We recently investigated the neural basis of odor recognition in young and elderly adults (Royet et al., 2011) by exploring correct (Hit) and incorrect (false alarms, FA) recognition and correct (CR) and incorrect (Miss) rejection. To characterize the brain responses in terms of functionally connected systems, we examined the functional relationships between the main regional foci using multivariate analyses of covariance and canonical variate analyses. We observed that significant activity in the hippocampus and parahippocampal gyrus was associated with correct recognition of odors. In this study, we go a step further by incorporating graph theory to study the differences between the networks underpinning correct and incorrect olfactory memories and to demonstrate how the brain areas composing these networks interact with each other.

Graph theory is used to quantify the overall properties of any system that can be described as a graph, *i.e.*, a set of nodes and a set of edges representing interactions between nodes. Graph theory has been widely applied to research fields as varied as biology, sociology, and technology science (Barabási, 2003; Newman et al., 2006) and, more recently, to brain data (Bullmore and Sporns, 2009). Graph theory has been used in fMRI to analyze both resting-state functional data (e.g., Achard et al., 2006; Achard and Bullmore, 2007) and task-related data (Shinkareva et al., 2008; Wang et al., 2010; Bassett et al., 2011; Ginestet and Simmons, 2011; Park et al., 2012).

Among several analyses derived from graph theory, modular decomposition aims at partitioning a network into several modules (also referred to as communities or clusters). Modules are characterized by nodes that work tightly together and less tightly with nodes belonging to other

modules (Newman and Girvan, 2004). Modular decomposition is achieved by maximizing a quality function, called modularity, and by assessing how well the nodes fit to modules of a given partition of the network. Modular decomposition has previously been applied to resting-state fMRI (Chen et al., 2008; Fair et al., 2009; Meunier et al., 2009a; Power et al., 2012; Stevens et al., 2012).

Several limitations of modular analysis can result in a loss of information. First, computing modularity over a range of thresholds may lead to issues concerning the independence of the considered samples (Langer et al., 2013). Second, modular analysis considers only positive correlations, which is inadequate for functional connectivity analysis because anti-correlated sub-systems can work in opposition to each other (Fox et al., 2005). Third, statistical comparisons of graphs obtained from different experimental conditions is not straightforward, although some methods have been proposed to compare modular structures between two groups of subjects when data were acquired in the resting-state (Alexander-Bloch et al., 2012; Moussa et al., 2012).

In this article, we investigated the functional networks involved in olfactory recognition memory. We overcame the limitations previously described by using modularity quality functions for weighted and signed graphs (Gómez et al., 2009; Traag and Bruggeman, 2009). We developed statistical validation methods using similarity-based tests to assess the significance of differences obtained at the modular level between young and elderly adults and between the four memory response categories (Hit, FA, CR, and Miss). We further correlated the modularity values with the behavioral performance of the subjects.

Materials and Methods

The methodology was reported in detail previously (Royet et al., 2011) and is briefly described here. Only the distinct aspects are extensively described in the present study.

Experimental task and behavioral analysis

Subjects

A total of 16 young [7 men; age: 27.14 ± 5.27 years (mean ± SD); range: 21.90-37.30] and 22 elderly (11 men; age 68.64 ± 3.29 years; range: 65.00-74.76) right-handed subjects participated in the study. This experiment was conducted in accordance with the Declaration of Helsinki. All subjects provided written informed consent as required by the local Institutional Review Board according to French regulations on biomedical experiments with healthy volunteers [Ethical Committee of CPP-Sud Est II (n CPP A 06-024), DGS2006-0226, May 11, 2006].

Stimuli and experiment

Subjects participated in a classical olfactory memory recognition task initially proposed by Engen and Ross (1973). A total of 100 odorants were used, comprising 50 target (old) and 50 distractor (new) odorants. Stimuli were counterbalanced by quality and mean scores of intensity, hedonicity, and familiarity obtained from previous data (Royet et al., 1999). The odorants were presented using an airflow olfactometer, which allowed the stimuli to be synchronized with breathing (Vigouroux et al., 2005). Odorants were delivered through a standard oxygen mask positioned on the subject's face.

Two functional runs corresponding to encoding and retrieval sessions were performed, separated by the structural image acquisition sequence. The 50 target odorants were presented in the encoding session and then interleaved with the 50 distractor odorants in the retrieval session. Odorants were delivered according to an event-related fMRI design with a jittered interstimulus interval of ~15 s, depending on the participant's respiration. The order of presentation of the odorants was randomized between participants for both sessions. During the encoding session, participants

indicated when they detected an odorant by pressing one button with their right hand. Participants were not instructed about the objective of the next session. During the retrieval session, the participants indicated whether or not they had already smelled the odorant in the first session.

Behavioral data analysis

Recognition memory performance was assessed using parameters issued from signal detection theory (Lockhart and Murdock, 1970). Hit, Miss, CR, and FA response categories were assigned based on the experimental conditions (old or new odorants) and the subjects' behavioral answers (yes or no). Two parameters were calculated from the Hit and FA scores: a memory score (d'_L) and a response bias score (C_L). Corwin (1989) previously described these calculations as follows:

$$d'_L = \ln \frac{HR(1-FR)}{FR(1-HR)} \quad (1)$$

$$C_L = 0.5 \times \ln \frac{(1-FR)\,(1-HR)}{(HR \times FR)} \quad (2)$$

where HR represents the Hit rate [(N_{Hit} + 0.5) / (N_1 + 1)], FR represents the false-alarm rate [(N_{FA} + 0.5) / (N_2 + 1)], and N_1 and N_2 represent the number of old and new odorants, respectively, for which the subjects provided an answer. As $N_1 = N_{Hit} + N_{Miss}$, and $N_2 = N_{CR} + N_{FA,}$ information about all 4 response categories are included in both d'_L and C_L. The memory scores were good or poor (positive and negative values, respectively). The response bias scores established three individual attitudes. Subjects could be conservative (tending to respond "no" to an odor), neutral (responding "yes" or "no" with equal probability), or liberal (tending to respond "yes") (Snodgrass, 1988), corresponding to positive, null or negative values, respectively.

Image acquisition

Images were acquired with a 1.5-Tesla MAGNETOM Sonata whole-body imager (Siemens medical®, Erlangen, Germany) equipped with a 4-channel circularly polarized head coil. For functional imaging, we obtained 26 interleaved 4-mm-thick axial slices using a T2*-weighted echo-planar sequence with the following parameters: repetition time (TR) = 2500 ms, echo time (TE) = 50 ms, flip angle = 80°, file-of-view (FOV) = 240 x 240 mm, and imaging matrix = 64 x 64 (voxel

size: 3.8 x 3.8 x 4 mm). We collected 324 scans for the encoding session and 624 scans for the retrieval session. Between functional sessions, a high-resolution structural T1-weighted anatomical image (inversion-recovery 3D Gradient-Echo sequence, 1 x 1 x 1 mm) parallel to the bicommissural plane and covering the entire brain was acquired over ~10 min.

fMRI data pre-processing and classical parametric statistical analyses

Functional images were pre-processed using Statistical Parametric Mapping software (SPM2, Wellcome Department of Cognitive Neurology, London, UK) (Friston et al., 1995). Images were spatially realigned, slice-time corrected, normalized, and smoothed with an 8-mm kernel. Pre-processed data were then statistically analyzed using a random-effects model. Regressors of interest, including the five experimental conditions of interest (Hit, FA, CR, Miss, and non-answer), were modeled using boxcar predictors convolved with both the canonical hemodynamic response function (hrf) and its time-derivative (Friston et al., 1998; Hopfinger et al., 2000).

Random-effects analyses were performed to extrapolate statistical inferences at the population level. Voxel-by-voxel single sample *t*-tests were performed for the response categories [Hit], [FA], [CR], and [Miss] to highlight activation that differed significantly from zero. To distinguish areas preferentially activated as a function of the four response categories and both groups, 12 *t*-contrast maps were calculated by comparing the Hit, FA, CR, and Miss items to each other, *i.e.*, [Hit *vs.* FA], [Hit *vs.* CR], [Hit *vs.* Miss], [FA *vs.* CR], [FA *vs.* Miss], and [CR *vs.* Miss], in both directions. The anatomic atlases created by Duvernoy and Bourgouin (1999) and Mai et al. (2008) were used to localize and describe activated brain regions. We kept uncorrected values at $p < 0.005$ and used an extent threshold greater or equal to five adjacent activated voxels. In addition, specific analyses were performed on brain regions known to play a role in olfactory and memory processing. Anatomical Volumes-Of-Interest (VOIs) were manually drawn from the MNI template using MRIcro (http://www.mricro.com) and the human brain atlases (Duvernoy and Bourgouin, 1999; Mai et al., 2008).

Modular structure analyses

VOIs selection and time-series extraction

We were interested in studying whether the brain areas identified as significantly activated during odor recognition (Royet et al., 2011) were organized as a network structure. Considering all possible contrasts, we identified a network of 22 structures in young subjects and 22 other structures in elderly participants for which activations (beta values) were significant. Among these structures, two anatomical VOIs (the right piriform and left perirhinal cortices) were common to both groups. Thus, 42 different structures (40 clusters + 2 anatomical VOIs) were considered in total. Because areas must be sufficiently spatially distinct, we considered two clusters identical when the interval between the coordinates of their activation peaks was less than 8 mm in a given direction. In this case, a new area with mean coordinates was considered instead of both original clusters. As a consequence, a set of 36 out of 42 structures was considered for subsequent analyses (Table 1; see also Supplementary Figure S1). This network represents only a part of the whole brain functional network but focuses on areas that specifically contributed to our task, i.e. the correct and incorrect recognitions and rejections of odors. From the activation peaks, cubes with a length of 8 mm were defined, and raw time series averaged over the voxels within a cube were extracted using the MarsBar toolbox (http://marsbar.sourcefourge.net) for each of the 38 participants. Head movement parameters (rotation and translation) were regressed, and residuals were high-pass filtered (> 0.01 Hz) to remove the scanner drift component of the signal and normalized (Z-score) for each session.

Table 1
List of 36 brain structures used for analyses, with corresponding abbreviations and coordinates (x y z).

N°	Brain structure	Abbreviation	MNI Coordinates x y z
1	Anterior cingulate	aCing	15 4 28
2	Angular gyrus	Ang1	53 -57 40
3	Angular gyrus	Ang2	-46 -61 32
4	Angular gyrus	Ang3	-27 -57 40
5	Caudate nucleus	Caud	-15 27 4
6	Cerebellum	Cere	40 -45 -30
7	Hippocampus	Hip1	-30 -38 0
8	Hippocampus	Hip2	19 -23 -12
9	Inferior frontal gyrus	IFg1	34 23 8
10	Inferior frontal gyrus	IFg2	44 21 22
11	Inferior frontal gyrus	IFg3	49 19 4

12	Inferior lingual gyrus	Iling	-4 -78 -12
13	Insula	Ins	27 19 8
14	Lateral orbital gyrus	Log	38 27 -4
15	Middle frontal gyrus	MFg1	-23 27 40
16	Middle frontal gyrus	MFg2	42 -8 48
17	Middle orbital gyrus	Mog	-42 -80 8
18	Middle temporal gyrus	MTg1	-42 -38 0
19	Middle temporal gyrus	MTg2	57 -67.5 0
20	Middle temporal gyrus	MTg3	49 -49 8
21	Posterior cingulate gyrus	pCing	4 -46 20
22	Paracentral lobule	PCL1	0 -42 56
23	Paracentral lobule	PCL2	11 -27 52
24	Precuneus	Pcun	11 -57 36
25	Perirhinal gyrus	Peri	-22 0 -34
26	Parahippocampal gyrus	PHg	-30 -34 -12
27	Posterior piriform cortex	pPC	15 4 -14
28	Precentral gyrus	Prec	-46 -16 36
29	Putamen	Puta	23 0 4
30	Superior frontal gyrus	SFg1	-6 -2 51
31	Superior frontal gyrus	SFg2	8 4 48
32	Superior lingual gyrus	Sling	11 -72 -4
33	Supramarginal gyrus	SMg1	53 -42 40
34	Supramarginal gyrus	SMg2	-61 -46 36
35	Thalamus	Tha1	-14 -4 -1
36	Thalamus	Tha2	12 -8 -2

MNI, Montreal Neurological Institute

Condition-based correlation matrices

To compute condition-based correlation matrices, we used the procedure described by Dodel et al. (2005). The specific regressors for each condition (*i.e.*, the set of trials that were identified as belonging to a given condition on the basis of the subject's response) were considered and convolved with a canonical hrf. Only the positive and null parts of the hrf were considered and used to compute weighted correlations of VOI structure time-series pairs. This resulted in a set of correlation matrices (36*36) for each one of the four response categories (Hit, FA, CR, and Miss).

Weighted Signed Modularity

In studies of modular structures in complex networks, modular decomposition is achieved by identifying the graph partitioning that optimizes a quality function known as modularity (Fortunato, 2010). Initially, the quality function of modularity was defined for binary graphs (Newman and Girvan, 2004). However, applying such a method to correlation matrices, as usually conducted for fMRI data, raises several issues.

First, the choice of a threshold over positive correlation coefficients to obtain binary links is

often arbitrary. One solution to this problem is to study network properties over a range of thresholds, but the problem of independency then arises for statistical validation (Langer et al., 2013). Another solution is to use modular decomposition while retaining the information of the value of each correlation coefficient by using modular decomposition of weighted graphs (Newman, 2004). For a weighted graph G composed of N nodes and a weighted matrix W, with w_{ij} defining the strength of the edge between nodes i and j, the optimization process aims to maximize the quality value Q, which reflects the goodness of a given partition $\{C_i\}_{i\in\{1,\ldots,N\}}$:

$$Q = \frac{1}{2w}\sum_i\sum_j (w_{ij} - \frac{w_i w_j}{2w}) \times \delta(C_i, C_j) \qquad (3)$$

where w is the total weight over all edges in the graph; w_i is the sum of weights of edges that include node i; C_i is the module index whose node i belongs to; and δ is the Kronecker function $\delta(a,a) = 1$ and $\delta(a,b) = 0$, if $a \neq b$. This measure of the modularity is based on the difference between weights joining nodes within the same module and the expected value of these same weights when they are distributed randomly between nodes.

Second, negative values of a correlation coefficient are sometimes considered as positive values because some computations consider absolute values (Achard et al., 2006; Meunier et al., 2009a). However, in resting-state fMRI, subsystems may be anti-correlated with each other (Fox et al., 2005), and considering the sign of correlations in graph analysis permits the segregation of anti-correlated subsystems (Rubinov and Sporns, 2011). In addition, negative correlations between activities also play a strong role in explaining cognitive processes (Chaminade and Fonlupt, 2003; Caclin and Fonlupt, 2006; Kelly et al., 2008). Therefore, it is crucial to consider the sign of correlation coefficients. Recently, Gómez et al. (2009) and Traag and Bruggeman (2009) proposed a reformulation of modularity that enabled the analysis of modular structure in complex networks with weighted and signed links. The idea behind this extension is that a partition in a set of modules is relevant when modules gather nodes between which there are mostly positive correlations and when nodes belonging to different modules are negatively correlated. Two different quality

functions are computed by considering the networks of positive and negative values separately:

$$Q^{+} = \frac{1}{2w^{+}} \sum_{i} \sum_{j} (w_{ij}^{+} - \frac{w_i^{+} w_j^{+}}{2w^{+}}) \times \delta(C_i, C_j) \quad (4)$$

$$Q^{-} = \frac{1}{2w^{-}} \sum_{i} \sum_{j} (w_{ij}^{-} - \frac{w_i^{-} w_j^{-}}{2w^{-}}) \times \delta(C_i, C_j) \quad (5)$$

where w_{ij}^{+} is max(0,*wij*) (resp. w_{ij}^{-} is max(0,-w_{ij})); w_i+ is the sum over all w_{ij}^{+}, including node *i* (resp. w_i^{-} is the sum over all w_{ij}^{-} including node *i*); and w^{+} if the total of all w_{ij}^{+} in the graph (resp. w^{-} if the total of all w_{ij-} in the graph). The quantity to maximize according to this principle is then obtained by weighting the difference of modularity for the positive and negative parts of the network:

$$Q = \frac{2w^{+}}{2w^{+} + 2w^{-}} Q^{+} - \frac{2w^{-}}{2w^{+} + 2w^{-}} Q^{-} \quad (6)$$

Modular decomposition is applied on each subject x condition-based correlation matrix. Modular decomposition was computed using a greedy algorithm from (Clauset et al., 2004), modified to take into account weighted signed modularity. Greedy algorithm has been shown to provide a good trade-off between time of computation and quality of the optimal partition (Blondel et al., 2008). Because even random networks may have a non-zero value for modularity (Guimerà et al., 2004), the values of the original networks must be compared with those of equivalent random networks obtained by randomly permuting values in the original matrices. Symmetry is conserved in the permutation process, and we ensured that each link was permuted with another link exactly once for every equivalent random network. We computed modularity on 100 randomized networks for each of the (16+22 subjects) x 4 (response categories) correlation matrices. We provided *p*-values, as assessed as the number of times a randomized networks achieved a higher modularity value than the original network, divided by the total number of randomized networks (most significant *p*-value is 0.01).

Individual modular partitions can be represented as binary co-classification matrices that have a value of one when two nodes belong to the same module. To assess a representative structure of a

given condition for a group of subjects, a mean co-classification matrix can be computed by averaging binary co-classification matrices (Sales-Pardo et al., 2007). The statistical reliability of a given subset of nodes of interest can be tested *a posteriori* by computing a normalized co-classification density for each subject. This is achieved by first considering, for a given subject, the number of times two nodes belonging to a subset are co-classified out of all the pairs involving the nodes in the subset. This quantity is then normalized by the total number of co-classified pairs for the subject.

N-uplets

Although co-classification matrices are useful for representing average modular structures for a given condition, these matrices should not be misinterpreted. The areas of pairs A-B and A-C may be co-classified, but the triplet of areas A-B-C may not occur as frequently in the same module. To verify the shared belonging of co-classified node pairs, individual co-classification matrices were also employed to assess how frequently three nodes (triplets), four nodes (quadruplets), and five nodes (quintuplets) were found in the same module. These N-uplets were considered relevant and could be displayed when they were observed in 50% of the subjects within a group for a given response category. If a given N-uplet was found in more than 50% of the subjects, we indicated the exact percentage value in the text (see Supplementary Material).

Normalized Mutual Information

Similarity measures were used to assess differences between partitions obtained for different individuals and experimental conditions. For graph G (containing N nodes), we considered two partitions A and B, each of which contain c_A and c_B modules, respectively. Each module in A is denoted A_i, $i \in 1,..., cA.$.

Normalized Mutual Information (NMI), a similarity measure based on information theory (Danon et al., 2005), requires the definition of a confusion matrix M. The term $m_{ij} = |A_i \cap B_j|$ represents the number of nodes in common between the communities A_i and B_j. The sum over the

row *i* of matrix *M* is denoted m_i and the sum over the column *j* is denoted m_j. NMI is defined as follows:

$$NMI(A,B) = \frac{\sum_{i=1}^{C_A}\sum_{i=1}^{C_B} m_{ij}\log\left(\frac{m_{ij}N}{m_i m_j}\right)}{\sum_{i=1}^{C_A} m_i \log\left(\frac{m_i}{N}\right) + \sum_{i=1}^{C_B} m_j \log\left(\frac{m_j}{N}\right)} \quad (7)$$

If the two partitions are identical, the *NMI* value is maximum and equal to 1. If the partitions are totally independent, the *NMI* value is null.

Statistical validation

Similarity measures were computed between pairs of partitions obtained for the same response category in different subjects or between pairs of response categories obtained for the same subject. We wanted to show the differences between age groups for the similarity values obtained for pairs of subjects belonging to the same population (young or elderly groups). Determining these differences raises several issues. First, a similarity measure computed with partitions *A* and *B* is not independent of a similarity measure computed with partitions *A* and *C* because partition *A* is involved in both cases. It is thus necessary to use statistical measures with no hypothesis on the independency of samples. Second, another level of dependency between the data arises as the measurements of the four response categories were obtained for each subject (repeated measurements).

Permutation tests and bootstrap methods are classically used to test differences in sets of dependent data (Good, 1994). However, their use for computing interactions in the non-parametric equivalent of two-way ANOVA remains controversial (Anderson and Ter Braak, 2003). In particular, it is unclear if the test should be computed on raw data (Manly, 1998) or on residuals after regression of both factors of interest (Ter Braak, 1992). Thus, interaction results computed with both raw data and residuals are presented in this study. Here, we chose to compute permutation tests by resampling subject-wise conditions (*i.e.*, the values for different response categories were not mixed between subjects), followed by resampling the subject age-group attributions to assess the effect of age. Each permutation was performed on 1000 randomly sampled tests, allowing a

maximum significance level of $\alpha = 0.001$ to be tested.

Pipeline of processing

A flowchart of processing steps including SPM pre-processing, SPM analysis, weighted correlation matrix, and modularity analysis was given in Supplementary Figure S2.

Results

Modularity values and statistical validation

Modularity values *Q* were computed for each correlation matrix representing a response category for a given individual, retaining both the sign and the value of the correlation coefficient. The modularity values showed neither an effect of age ($p > 0.3$) nor an effect of response category ($p > 0.2$). To demonstrate that the modularity values obtained for individual functional networks were different than the values obtained with equivalent random networks, we computed 100 simulations of randomized networks from each of 152 networks (38 subjects x 4 response categories) by permuting the values of two pairs chosen randomly until the values of all pairs had been permuted. The modularity values were computed for each simulation, and their mean and standard deviation were calculated. Each original modularity value was then transformed to a Z-score using the parameters obtained from the 100 equivalent random networks (Figure 1A). The percentage of functional networks displaying a significant non-random modularity value at a significance level α of 0.05 for all response categories is shown in Figure 1B for both age groups. The percentages ranged from 54 to 81% (mean = 71.6). The number of modules per subject ranged from 2 to 5 (mean = 2.88), and no effect of age ($F_{1,108} = 0.20$, $p = 0.66$) or response category ($F_{3,108} = 0.99$, $p = 0.400$) was observed.

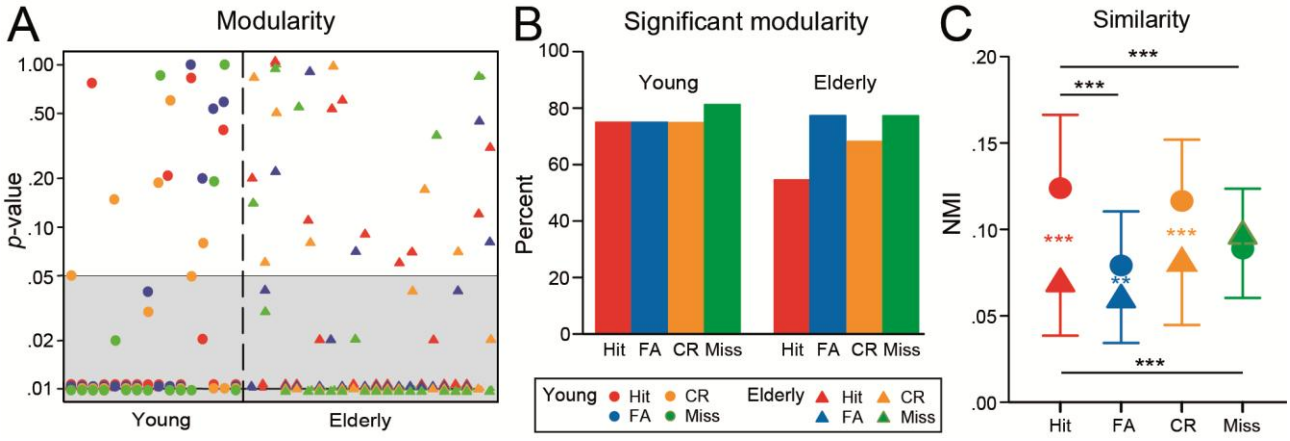

Figure 1. A) Probabilities that randomized networks achieved higher modularity values than the original network for the four response categories (Hit, FA, CR, and Miss) and for each of 16 young (circle) and 22 elderly (triangle) subjects; the grey area determines the limits for which modularity values were obtained with $p < 0.05$. At $p = .01$, markers of 4 response categories are slightly shifted

to be more distinct between them. B) Percentage of networks obtained for each response category and age group showing a significant positive Z-score of functional network modularity at a level of $\alpha = 0.05$. C) NMI similarity values as a function of response categories and age groups (means ± standard deviation). NMI, normalized mutual information.

The NMI similarity values calculated between partitions of all functional networks for response categories Hit, FA, CR, and Miss in young and elderly subjects are shown in Figure 1C. Permutation tests applied to raw data (Manly, 1998) revealed a significant main effect of age group ($p = 0.001$) and response category ($p = 0.001$) and a significant age group x response category interaction ($p = 0.001$). Permutation tests performed on residual data also showed a significant age group x response category interaction ($p = 0.001$). When considering the difference between response categories and taking each group independently, permutation tests revealed a significant effect of response categories in the young ($p = 0.001$) and elderly ($p = 0.001$) groups. Permutation tests further revealed significant differences between Hit and FA and between Hit and Miss in the young group ($p's = 0.001$). In elderly subjects, the mean value was significantly higher for Miss than for Hit, FA, and CR ($p's = 0.001$). Significant differences were also observed between young and elderly subjects for Hit ($p = 0.001$), FA ($p = 0.004$), and CR responses ($p = 0.001$).

Co-classification matrices

Once a modular partition was obtained for each correlation matrix, all resulting partitions were summarized by a mean co-classification matrix. Using a hierarchical clustering method (Ward, 1963), the nodes were reordered so that highly co-classified nodes were displayed close to each other, thus leading to a block diagonal matrix (Figure 2). For more details, see Supplementary Materials and Methods (hierarchical clustering). To facilitate comparisons between the eight matrices (4 response categories x 2 age groups), the matrices were reordered according to the order of the nodes (structures) obtained for the Hit condition in young subjects.

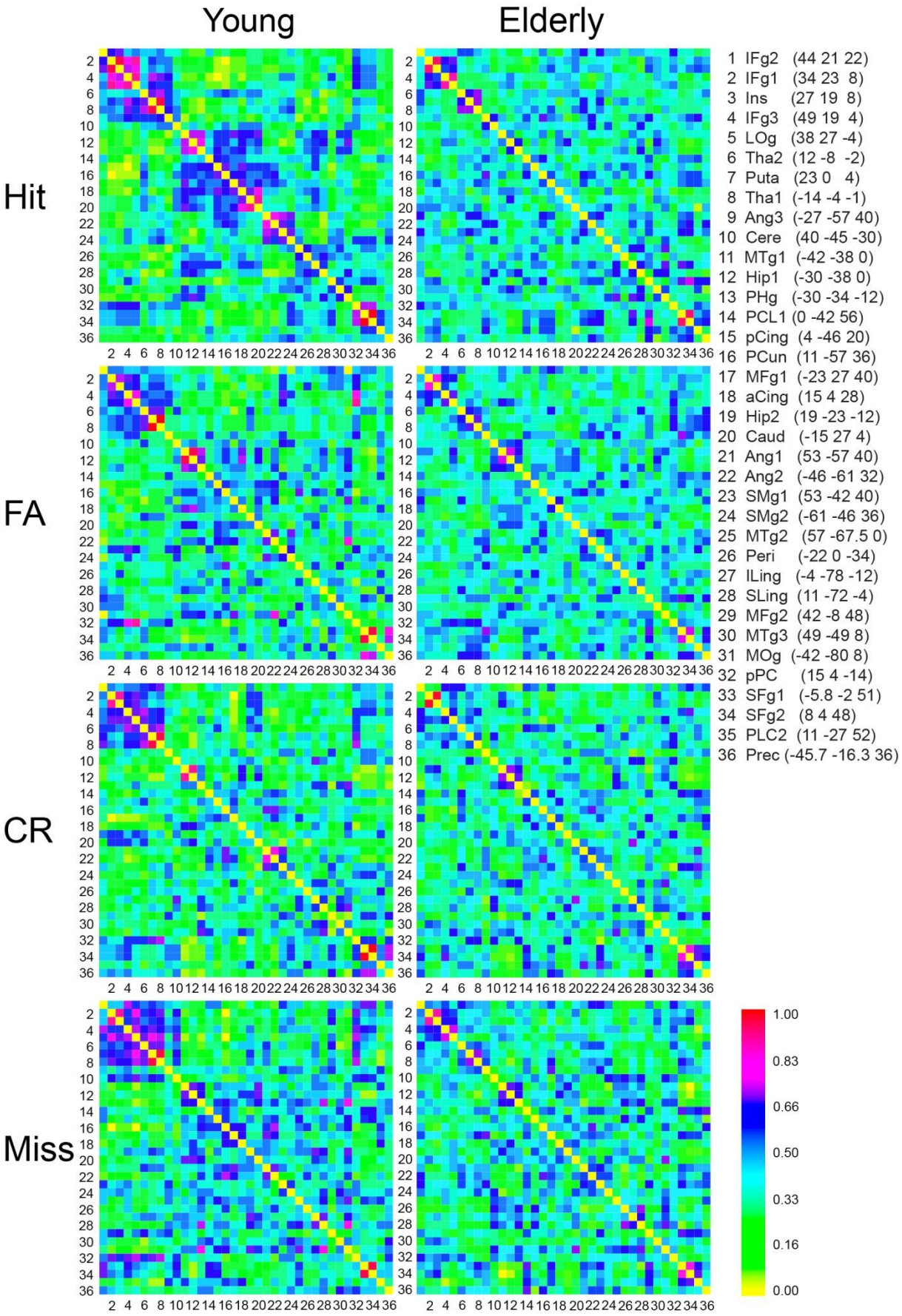

Figure 2. Mean co-classification matrices obtained for 36 structures for each response category (Hit, FA, CR, and Miss) in young and elderly subjects. The order of the structures in the matrices is based on that obtained for Hit in young subjects. Scale: percentage of individuals in the group in which a given pair of nodes belongs to the same module.

The mean co-classification matrices obtained for the young group were more heterogeneous than those calculated for the elderly group (Kruskal-Wallis test, $\chi^2 = 5.17$, $df = 1$, $p = 0.023$). The mean co-classification matrices in young subjects revealed a subset of nodes that were highly co-classified in the Hit condition but not in the FA, CR, and Miss conditions. This set of eight nodes (indexes 13-20 on Fig. 2) was composed of Hip2 (19 -23 -12), PHg (-12, -28, -10), aCing (15 4 28), pCing (4 -46 20), PCL1 (0 -42 56), PCun (11 -57 36), MFg1 (-23 27 40), and Caud (-15 27 4). MTg1 (index 11 on Fig 2) and Hip1 (index 12 on Fig. 2) were not part of this subset because they were also co-classified in the FA and CR conditions. We computed normalized co-classification densities for the eight structures as a function of the Hit, FA, CR, and Miss response categories (Figure 3). One-way ANOVA with repeated measures revealed a significant effect of response category ($F_{3,45} = 4.44$, $p = 0.007$), with co-classification indexes that were significantly denser for Hit than for FA (post-hoc Tukey HSD test, $p_{adjusted} = 0.048$), CR ($p_{adjusted} = 0.019$), and Miss ($p_{adjusted} = 0.027$) responses.

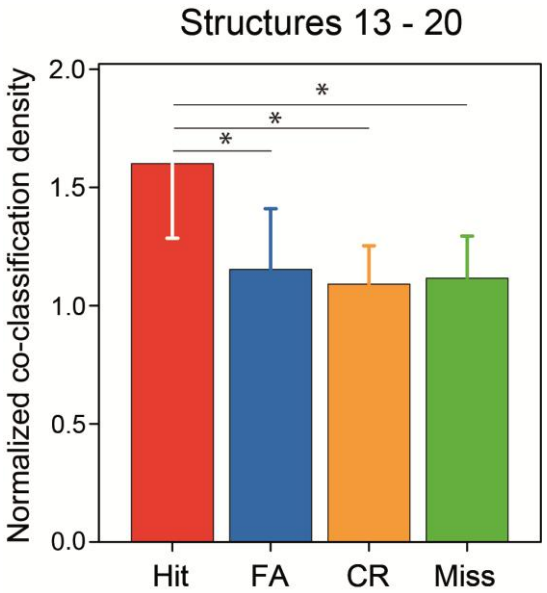

Figure 3. Mean normalized co-classification densities computed for eight structures (from indexes 13 to 20) in the Hit, FA, CR, and Miss conditions in young subjects. Vertical bars represent standard deviations. *, $p < 0.05$.

The mean co-classification matrices reordered according to the order of nodes obtained for the FA, CR, and Miss response categories are shown in Figures S3, S4, and S5, respectively. The reordered matrices did not reveal specific sets of nodes that were more significantly co-classified in

each of these response categories.

For sake of control, we further provided the co-classification matrices from data extracted during rest periods at the beginning of encoding and retrieval sessions, thus providing with several limitations the closest to 'resting-state' analysis (see sections "Functional connectivity analysis of rest periods" in Supplementary Materials and Methods, and Supplementary Results, and Supplementary Figure S6).

N-uplets and behavioral performance

Triplets and quadruplets (subsets of three or four nodes belonging to the same module in more than half of the subjects in a group) for the four response categories and the two age groups are shown in Figures S7 and S8, respectively. Overall, the number of triplets was higher in young than elderly subjects. For the Hit, FA, CR, and Miss response categories, we identified 36, 21, 22 and 50 triplets, respectively, in the young group and 20, 4, 7, and 15 triplets, respectively, in the elderly group. The number of quadruplets in young subjects was limited to 5 for Hit, 1 for FA, and 12 for Miss. No quadruplet was identified in elderly subjects.

Figure 4 focuses on the triplets and quadruplets for Hit and Miss in young subjects. In the Hit condition only, we found a triplet composed of Hip2, aCing, and Caud in 62.5% of the subjects. These same structures in association with MTg1 formed a quadruplet (in blue) in 56.25% of the subjects. Four other quadruplets were found: the first one (in green) was composed of LOg, IFg1, IFg3, and Ins (68.75% of the subjects); the second one (in light blue) associated LOg and IFg3 with Tha1 and Puta (50%); the third one (in cyan) joined Puta, Log, IFg1, and IFg3 (50%); and the last one (in purple) joined pPC, Ins, LOg, and IFg1 (50%). The quadruplet described above that was composed of Hip2, aCing, Caud, and MTg1 was also identified in three elderly subjects. We then determined that young and elderly subjects who presented this quadruplet had memory scores that were significantly higher than those of the subjects in which the four nodes did not belong to the same module ($t_{1,36} = 2.69$, $p = 0.011$).

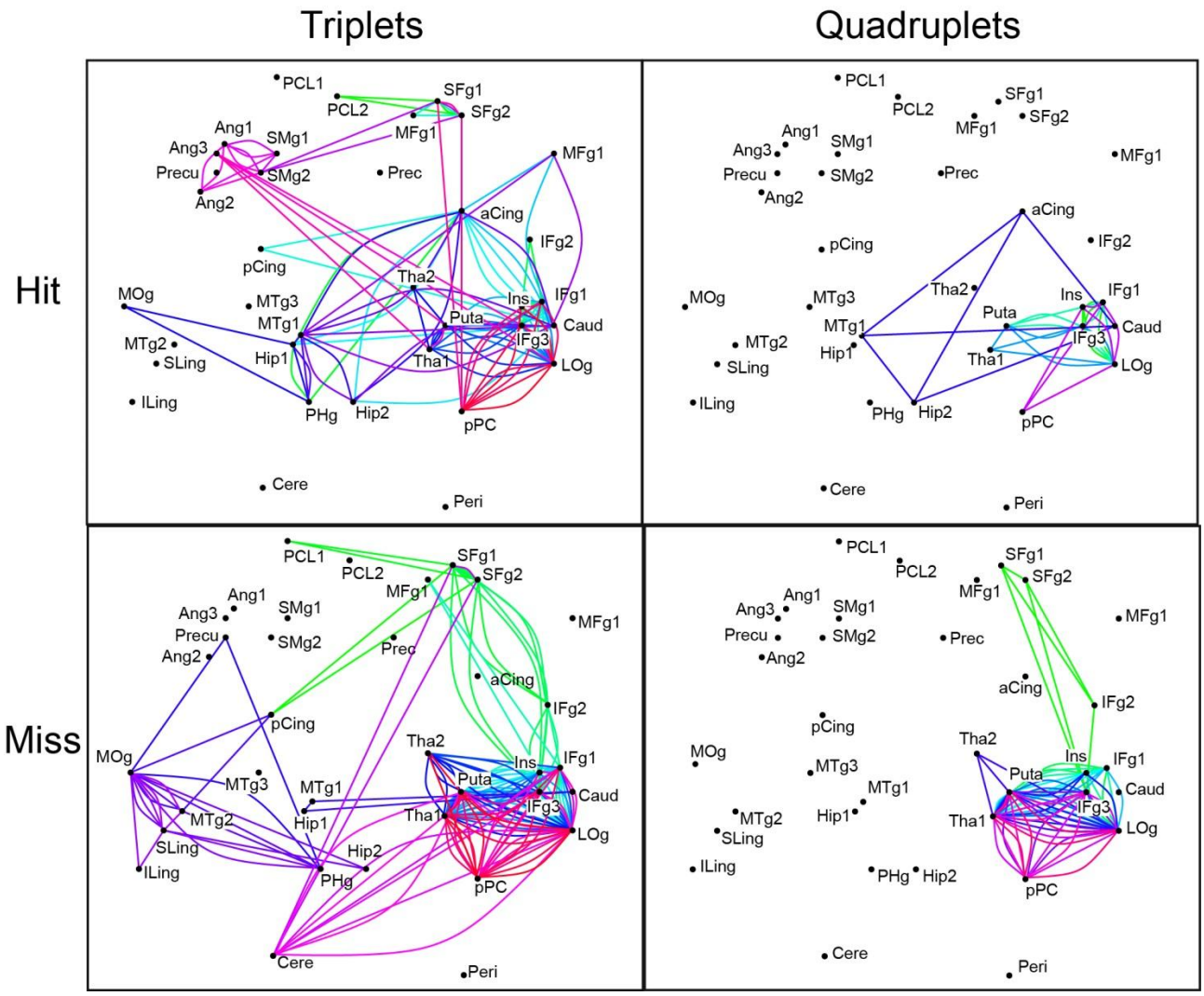

Figure 4. Spatial co-classification representations obtained for 36 structures when three (triplets) and four (quadruplets) nodes belong to the same module in the Hit and Miss conditions in young subjects. Links of the same color are drawn between nodes belonging to a similar N-uplet.

In the Miss condition for the young group, 10 of the 12 quadruplets were found between a subset of areas composed of Tha1, Puta, pPC, IFg1, IFg2, IFg3, Ins, and LOg. In addition to these areas (which were also connected, although less densely, in the Hit condition), an extra quadruplet (in green) included areas in the inferior and superior frontal gyri (IFg2, IFg3, SFg1, and SFg2). Another quadruplet (in blue) included two thalamus areas (Tha1 and Tha2) and Puta and LOg. We further determined that these structures [pPC, LOg, IFg1, IFg3, Ins, Puta, and Tha1] were particularly connected and formed two quintuplets in 50% of the subjects (see Figure S9). No other quintuplets were present in 50% of the subjects.

Correlations between modularity values and behavioral performances

We computed the correlations between the modularity values obtained for each subject in the Hit, FA, CR, and Miss response categories and memory scores (d'_L), and between the modularity values and bias scores (C_L). A significant negative correlation with memory scores (r = -0.44; p = 0.0052) was observed for the Hit condition only (Figure 5A). A trend effect of the CR condition was also noted (r = -0.30, p = 0.065). Strong significant positive correlations with bias scores were further observed for the Hit and FA responses (Figure 5B) (r = 0.62, p < 0.0001 and r = 0.51, p = 0.001, respectively).

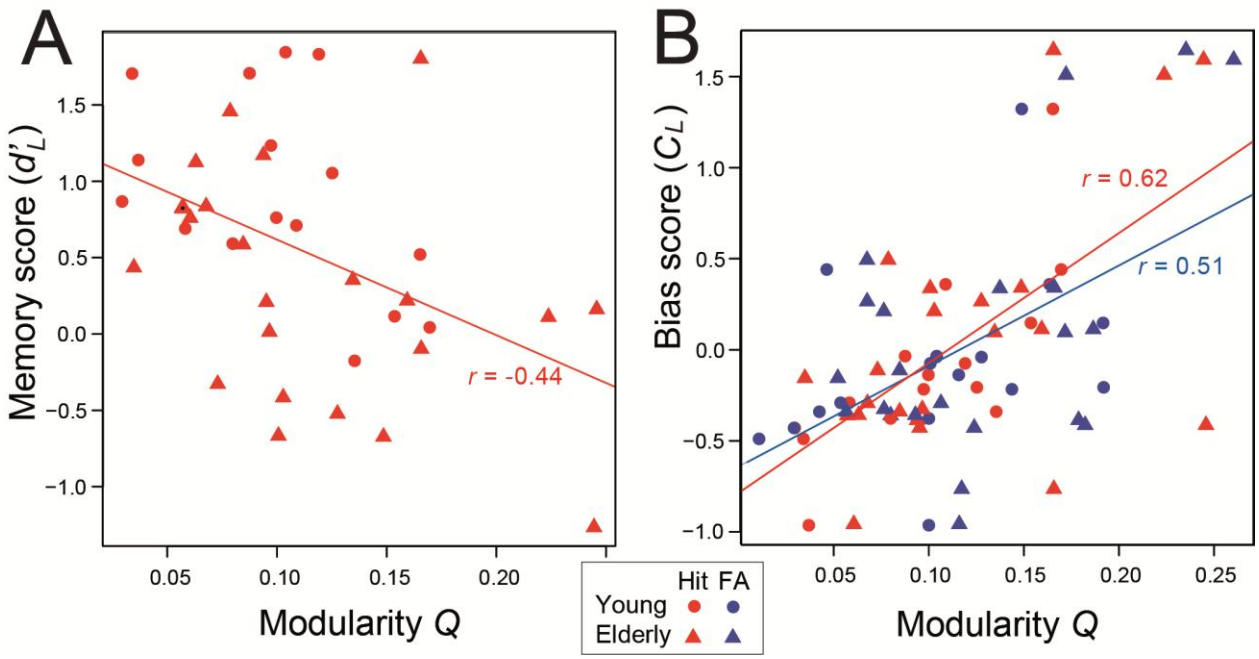

Figure 5. Correlations between modularity values (Q) and A) memory scores d'_L and B) bias scores C_L when subjects provided Hit (in red) or FA (in dark blue) responses. Individual values are represented by circles for young subjects and triangles for elderly subjects.

For each subject, we further computed the number of positive minus negative links between the modules, normalized by the total number of inter-module links. These data were negatively correlated with modularity values for all response categories taken together (r = -0.93; t_{150} = -31.6, $p < 10^{-15}$), confirming that the high modularity value was mainly due to an increased number of negative links. Correlating these values with behavioral scores, we then demonstrated that memory scores were positively correlated with the normalized number of positive minus negative links found in the Hit condition (r = 0.50, t_{36} = 3.46, p = 0.0014; Figure 6A) and that the bias scores were

negatively correlated with the normalized number of positive minus negative links in the Hit and FA conditions (Hit: r = -0.63, t_{36} = -4.92, $p < 10^{-5}$; FA: r = -0.45, t_{36} = -3.01, p = 0.0047; Figure 6B).

By way of illustration, we present examples of modular structures computed at the individual scale for extreme values of memory and bias scores (Figure 6). In the Hit condition, inter-modular links were almost exclusively positive when the memory score was high (subject 12, d'_L = 1.705) and partly negative when the memory score was very low (subject 20, d'_L = -1.266). In both Hit and FA, inter-modular links were exclusively positive when the bias scores were very low (subject 3 for Hit and FA, C_L = -0.967) and partly negative when bias scores were high (subject 28 for Hit, C_L = 1.505; and subject 32 for FA, C_L = 1.642).

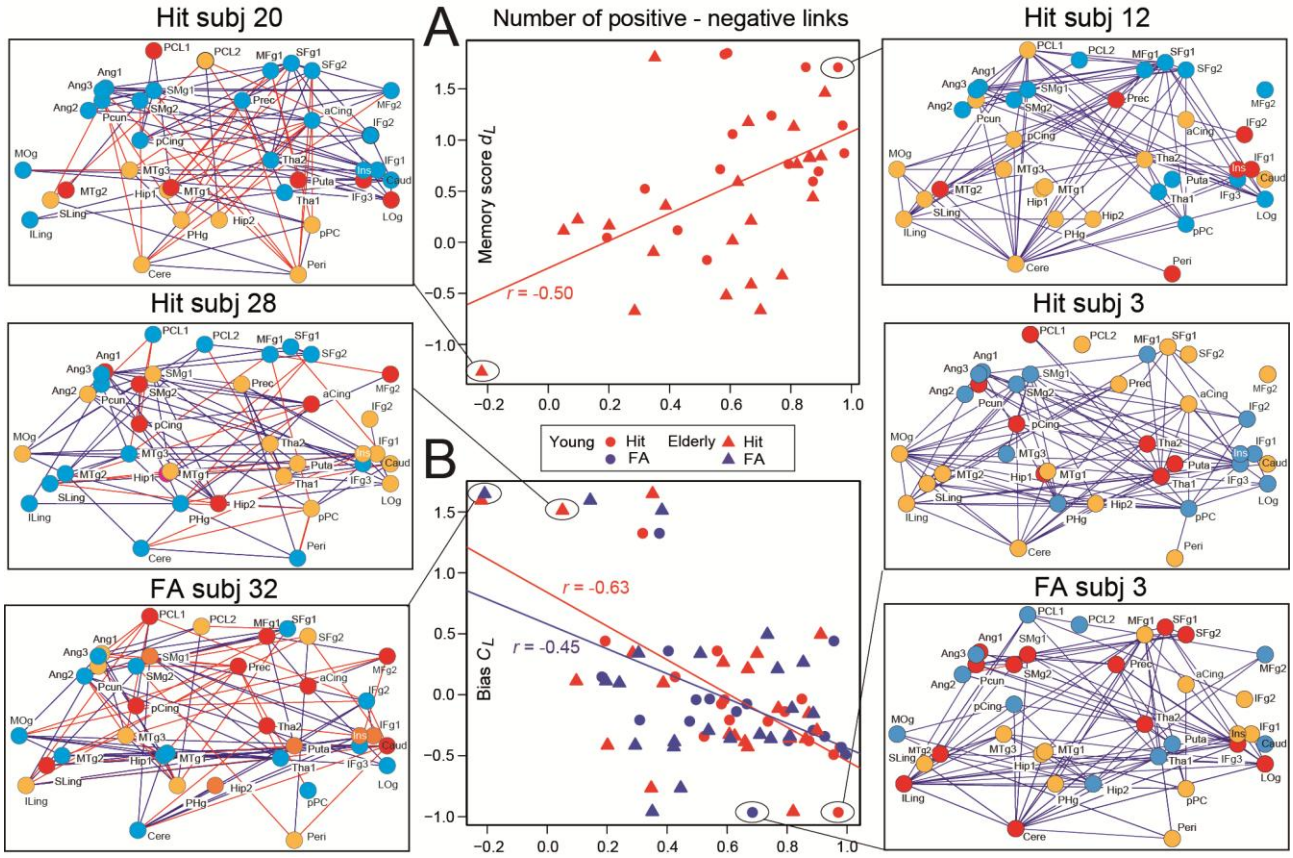

Figure 6. Correlations between the number of positive minus negative links between modules for each subject and A) memory scores d_L and B) bias scores C_L when subjects provided Hit or FA responses. Individual values are represented by circles for young subjects and triangles for elderly subjects and by red for the Hit condition and blue for the FA condition. Left and right sides: modular structures observed in four subjects for which memory or bias scores were the smallest or the strongest. Nodes are represented at the area coordinates given in Table 1. For each subject, nodes belonging to the same module are represented with the same color: yellow, orange, red, or blue. The same color does not indicate the same module for different subjects. The connections

corresponding to the first 100 highest correlations in absolute values are represented in blue or red according to whether nodes were positively or negatively correlated, respectively. Note that the connections are shown for representation purposes only; the modular decomposition was achieved using all correlation values with a weighted signed modularity algorithm.

Discussion

Several studies, particularly resting-state fMRI studies, have shown that functional networks at the whole brain level have a modular architecture (Fair et al., 2009; He et al., 2009; Meunier et al., 2009a; 2009b; Power et al., 2012). Hypotheses have been advanced to explain the benefits of modularity (Meunier et al., 2010), such as superior evolvability (Simon, 1962), the capacity to generate more complex dynamics (Shanahan, 2010), and better results when coping with different tasks simultaneously (Kashtan and Alon, 2005). The only study to provide some evidence that a task (working memory capacity) could influence the modular structure of functional networks was performed using resting-state fMRI (Stevens et al., 2012). To our knowledge, our study is the first to examine the modular structure of a neural network while the subjects were performing a specific cognitive task in the scanner. Here, we aimed to identify the modular structure of neural networks differentially involved in true and false odor recognition memory in young and elderly subjects. We proposed a new method that considers weighted and signed graphs and also developed statistical validation methods. We further validated and explained our modularity results by relating them to behavioral performance.

Modularity values, co-classification matrices, and specific N-uplets as a function of conditions

By applying modular decomposition algorithms, we were able to go beyond assigning a set of areas showing activation in specific contrasts as a "network", as it is usually observed in studies using general linear model. Instead, we quantified how much these areas were working specifically within a network. Permutation tests were applied to assess significant differences among NMI similarity values computed after modular decomposition. We determined that the similarity values were differently modulated across response categories (Hit, FA, CR, and Miss), and the two age groups (Figure 1C).

When comparing both groups, similarity values were significantly lower in elderly than young

subjects for Hit, FA, and CR, indicating that modular partitions in the elderly were less homogeneous than in young subjects. Concurrently, the patterns identified with co-classification matrices were more diffuse in elderly than young subjects for all response categories (Figure 2). This result may be explained by the fact that each elderly subject either used a personal strategy that was not representative of the group or answered at random for a portion of the trial due to an attention problem. In both cases, the neural networks involved in a given condition were likely not the same between the subjects. The results further showed that the subsets of highly co-classified nodes observed in the co-classification matrices obtained from rest period data were more diffuse (more heterogeneous) than those obtained for the task-related periods, thus providing some evidence that the task-related partitions were specific of the response categories. When considering the young subjects only, we observed an effect of response category on similarity values. The partitions obtained for the two response categories involving a correct memory process (Hit and CR) were more similar (*i.e.*, the neural networks were more homogeneous) across young subjects than for the two response categories involving an incorrect memory process (FA and Miss) (Figure 1C). In other words, there was one way to be right and several ways to be wrong. The co-classification matrices provided some evidence that some modules were conserved for all response categories, while some areas were specifically co-classified for a given response category. This was particularly the case in the Hit condition (Figure 2). Thus, we were able to demonstrate that a specific subset of eight areas (areas 13-20) comprising the parahippocampal gyrus (PHg), paracentral lobule (PCL1), posterior cingulate gyrus (pCing), precuneus (pCun), middle frontal gyrus (MFg1), anterior cingulate gyrus (aCing), hippocampus (Hip2), and caudate nucleus (Caud) was statistically more often included in a similar module (*i.e.*, they were working together in most subjects) during correct odor recognition (Hit) compared to other conditions. These results are of particular interest because these areas are known to be involved in recollection processes: hippocampal activity is reliably increased during retrieval for items that are recollected and is not modified for non-recollected items (Matthews and Gilliland, 1999; Savic et al., 2000; Stark and

Squire, 2000; Canli et al., 2001; Royet et al., 2001; Rose et al., 2002). Similar although less robust results were observed for the parahippocampal area (Canli et al., 2001; Kirwan and Stark, 2004; Eisenberger et al., 2005; Adelstein et al., 2011). In a meta-analysis study, Kim (2013) observed that the correct recognition of old items (Hit) versus the correct rejection of new items (CR) was consistently associated with several of the neural regions described above. The author categorized the regions into three types: the default-mode network (angular cortex, precuneus, and posterior cingulate cortex), which would support ecphory, *i.e.*, the mental re-experiencing of an old event; the cognitive-control network (dorsolateral and dorsomedial prefrontal cortices, intraparietal sulcus), which would mediate memory and non-memory control functions; and the caudate nucleus, which would support the satisfaction tied to target detection.

Among eight areas observed in young subjects for Hit responses, we further found that three areas, Hip2, aCing, and Caud, formed a specific quadruplet with the left MTg1 (Figure 4). The involvement of these three areas deserves some explanation. Recognition memory is not an 'all-or-none' process but varies in the degree of subjective confidence that an event has been previously experienced (Kim and Cabeza, 2009). It emerges from previous studies that, along the medial temporal regions, the anterior cingulate gyrus is associated with an increase in confidence at recognition (Chua et al., 2006; Moritz et al., 2006; Kim and Cabeza, 2009). Moritz et al. (2006) questioned whether confidence-related activation of this region may be associated with the role proposed by Rushworth et al. (2004) in "guiding decisions about which actions are worth making", particularly those involving reward expectancy (Shidara and Richmond, 2002; Matsumoto et al., 2003). They suggested this association because, in many contexts, high confidence can be equivalent to the promise of reward. Consistently, Guitart-Masip et al. (2013), using magnetoencephalography, demonstrated that mnemonic guidance of nonspatial human decision making, beyond anticipation of the expected reward, is supported by theta synchronization between the hippocampus and several prefrontal regions, including the dorsal anterior cingulate gyrus. Here, we further demonstrated that aCing is co-activated with the Caud, a structure playing a key role in

the reward system with adjacent striatal regions (Kim et al., 2008) and whose activation may reflect the reward or satisfaction of successful target detection (Rauch et al., 2005). The left MTg1 included in the quadruplet was excluded from our computations of mean co-classified indexes (Figure 3A) because it was also highly co-classified in the FA condition (index 11 on Figure 2). However, the finding that this area belonged to the same quadruplet for more than 56% of the young subjects (as well as three elderly subjects) highlights its crucial importance in the process of correct odor recognition. Indeed, subjects recruiting this quadruplet had significantly higher memory scores than those that did not. The left MTg1 was previously associated with the lateral intraparietal area during visual perceptual decision-making (Kayser et al., 2010).

Four other quadruplets connecting areas located in the inferior frontal gyri (IFg1 and IFg3), the lateral orbital gyrus (LOg), the insula (Ins), the posterior piriform cortex (pPC), the thalamus (Tha1), the putamen (Puta), and the Caud were found in the Hit condition. These areas are closely associated with odor information processing (*e.g.*, attention, semantics) (Savic et al., 2000; Royet et al., 2001; Gottfried and Zald, 2005; Zelano et al., 2005; Plailly et al., 2008) and have also been reported to play a role in reward-related decision-making (Balleine and O'Doherty, 2010; Liu et al., 2011). However, these quadruplets were not specific to the Hit condition because they were also found in the FA and Miss conditions. They were particularly interconnected in the Miss condition, revealing two quintuplets in half of the subjects. Another quadruplet was observed in the Miss condition, connecting several areas of the inferior and superior frontal gyri (SFg1, SFg2, IFg2, and IFg3).

Modularity and behavioral performance

We demonstrated that modularity is negatively correlated with memory scores (d'_L) in the conditions involving a correct response (Hit, with a trend for CR) but not in the other conditions. This result means that subjects with good memory scores involve functional networks that are less segregated than subjects with low memory scores. In fact, we determined that the number of modules was relatively stable (from 2 to 5), whatever the memory scores, but that the number of

positive minus negative links interconnecting modules was positively correlated with memory scores (Figure 6). In other words, the higher the memory scores, the more connected with positive correlations the modules were. Dehaene et al. (1998) proposed a hypothesis concerning the brain processes underlying effortful tasks such as the Stroop task. They showed by simulation that a unique global workspace composed of distributed neurons with long-distance connectivity can be mobilized in effortful tasks to interconnect multiple distributed and specialized areas when the modular perceptual, motor, memory, evaluative, and attentional processors do not suffice. Here, we observed that workspace neurons were present in each module, but we further observed that these modules were more or less positively or negatively intercorrelated depending on memory scores. When memory scores were high, modules were then positively correlated and usually included the specific quadruplet (Hip2, Caud, aCing, and MTg1).

The number of positive minus negative links between modules was also negatively correlated with bias measures (C_L) in the Hit and FA conditions. When facing a previously smelled odor, conservative subjects activated a set of modules that was more negatively interconnected than those activated in liberal subjects. This result was unexpected because it relates functional connectivity to the liberal or conservative attitudes of individuals, which reflects a trait of their personality. Several fundamental dimensions of personality have been proposed (Eysenck, 1967; Rose et al., 2002), including extraversion-introversion, which represents the degree to which an individual is outgoing and interactive with other people. Extraversion is correlated with the number of false alarms; in other words, extraverts adopt more liberal response criteria (Harkins and Geen, 1975; Rose et al., 2002). As initially proposed by Eysenck (1967), it is now acknowledged that dimensions of personality have biological bases (Matthews and Gilliland, 1999). Recent cerebral imaging studies have demonstrated the differential involvement of brain structures as a function of personality dimensions (Canli et al., 2001; Eisenberger et al., 2005; Rauch et al., 2005; Kim et al., 2008), including functional connectivity studies based on resting-state and/or graph theoretical analysis (Adelstein et al., 2011; Gao et al., 2013).

Limitation of modularity analyses

Modularity optimization has a resolution limit that may prevent it from detecting modules which are comparatively small with respect to the graph as a whole, even when they are well defined modules like cliques (Fortunato and Barthelemy, 2007). This limit is also true when weighted modularity algorithms (Berry et al., 2011) are used, but is more problematic for very large graphs (e.g. web graphs), as pointed out by Fortunato (2010). Due to the small size of the graphs considered here (36 nodes), missing the detection of modules composed of 2 or 3 nodes does not appear as a real issue.

Another limitation is that a large value for the modularity maximum does not necessarily mean that a graph has a modular structure. Random graphs are supposed to have no modular structure, so there is a priori no bias towards special groups of nodes. Still, random graphs may have partitions with large modularity values (Guimerà et al., 2004; Reichardt and Bornholdt, 2006). This problem is due to fluctuations in the distribution of edges in the graph, which is not homogeneous even if the linking probability is constant as in Erdos-Renyi graphs (Fortunato, 2010). We have tried to tackle this limitation by computing permutations on each of the correlation matrices, thus disrupting any underlying structure, and testing the significance of the original correlation matrix.

Another caveat is the difficulty to find the optimal partition using heuristics. This is particularly observed when the highest modularity values are composed of a plateau of relatively close values, each corresponding to different, close to optimum, partitions of the network (Good et al., 2010).

All of our results have to be interpreted with these limitations in mind. As for any new analysis, the physiological relevance of the functional networks of olfactory memory would need replications based on similar or related protocols and involving other related clustering techniques (e.g. spectral or hierarchical clustering techniques).

Conclusions

We innovatively applied modular decomposition in the frame of a cognitive task, odor

recognition memory. We used, for the first time, a modularity quality function for weighted and signed graphs, allowing us to retain information about positive and negative correlations between structures. We further developed statistical methods to validate our results and correlated modularity values with behavioral performance. We demonstrated that 1) the functional networks during an odor recognition memory task are modular; 2) modular partitions of functional connectivity were more homogeneous in young than elderly subjects; 3) in young subjects, partitions were more homogeneous for correct recognition memory (Hit, CR) than for incorrect recognition memory (Miss, FA); 4) the Hit responses of subjects were concomitant with the activation of a module, including a set of eight specific areas (particularly the quadruplet of the hippocampus, caudate nucleus, and anterior cingulate and middle temporal gyri); 5) during a Hit, the higher the memory score, the more connected with positive correlations the modules were; 6) during a yes response (Hit or FA), the higher the bias score, the less connected with positive correlations the modules were: links were mainly positive when subjects were liberal and mainly negative when they were conservative. In brief, we provided evidence that the modular structure of functional networks is related to memory performance and personality traits.

Acknowledgements

This work was supported by the Centre National de la Recherche Scientifique (CNRS) and the LABEX Cortex (NR-11-LABX-0042) of Université de Lyon within the program "Investissements d'Avenir" (ANR-11-IDEX-0007) operated by the French National Research Agency (ANR). David Meunier was funded by LABEX Cortex. We thank the editors of American Journal Experts for careful review of the English of the manuscript.

References

Achard, S., Salvador, R., Whitcher, B., Suckling, J., Bullmore, E., 2006. A Resilient, Low-Frequency, Small-World Human Brain Functional Network with Highly Connected Association Cortical Hubs. J. Neurosci. 26**,** 63-72.

Achard, S., Bullmore, E., 2007. Efficiency and cost of economical brain functional networks. PLoS Comput Biol 3**,** 174-183.

Adelstein, J.S., Shehzad, Z., Mennes, M., Deyoung, C.G., Zuo, X.N., Kelly, C., Margulies, D.S., Bloomfield, A., Gray, J.R., Castellanos, F.X., Milham, M.P., 2011. Personality is reflected in the brain's intrinsic functional architecture. PLoS One 6**,** e27633.

Alexander-Bloch, A., Lambiotte, R., Roberts, B., Giedd, J., Gogtay, N., Bullmore, E., 2012. The discovery of population differences in network community structure: New methods and applications to brain functional networks in schizophrenia. NeuroImage 59**,** 3889-3900.

Anderson, M., Ter Braak, C., 2003. Permutation tests for multi-factorial analysis of variance. J. Stat. Comp. Simul. 73**,** 85-113.

Balleine, B.W., O'Doherty, J.P., 2010. Human and rodent homologies in action control: corticostriatal determinants of goal-directed and habitual action. Neuropsychopharmacol 35**,** 48-69.

Barabási, A.-L., 2003. Linked : how everything is connected to everything else and what it means for business, science, and everyday life, Plume, New York.

Bassett, D.S., Wymbs, N.F., Porter, M.A., Mucha, P.J., Carlson, J.M., Grafton, S.T., 2011. Dynamic reconfiguration of human brain networks during learning. Proc. Natl. Acad. Sci. USA 108**,** 7641-7646.

Berry, J.W., Hendrickson, B., LaViolette, R.A., Phillips, C.A., 2011. Tolerating the community detection resolution limit with edge weighting. Phys Rev E Stat Nonlin Soft Matter Phys 83**,** 056119.

Blondel, V.D., Guillaume, J.-L., Lambiotte, R., Lefebvre, E., 2008. Fast unfolding of communities in large networks. Journal of Statistical Mechanics: Theory and Experiment 2008**,** P10008.

Bullmore, E., Sporns, O., 2009. Complex brain networks: graph theoretical analysis of structural and functional systems. Nat. Rev. Neurosci. 10**,** 186-198.

Caclin, A., Fonlupt, P., 2006. Functional and effective connectivity in an fMRI study of an auditory-related task. Eur. J. Neurosci. 23**,** 2531-2537.

Calhoun, V.D., Adali, T., McGinty, V.B., Pekar, J.J., Watson, T.D., Pearlson, G.D., 2001. fMRI activation in a visual-perception task: network of areas detected using the general linear model

and independent components analysis. Neuroimage 14**,** 1080-1088.

Canli, T., Zhao, Z., Desmond, J.E., Kang, E., Gross, J., Gabrieli, J.D., 2001. An fMRI study of personality influences on brain reactivity to emotional stimuli. Behav. Neurosci. 115**,** 33-42.

Chaminade, T., Fonlupt, P., 2003. Changes of effective connectivity between the lateral and medial parts of the prefrontal cortex during a visual task. Eur. J. Neurosci. 18**,** 675-679.

Chen, Z.J., He, Y., Rosa-Neto, P., Germann, J., Evans, A.C., 2008. Revealing Modular Architecture of Human Brain Structural Networks by Using Cortical Thickness from MRI. Cereb. Cortex 18**,** 2374-2381.

Chua, E.F., Schacter, D.L., Rand-Giovannetti, E., Sperling, R.A., 2006. Understanding metamemory: neural correlates of the cognitive process and subjective level of confidence in recognition memory. Neuroimage 29**,** 1150-1160.

Clauset, A., Newman, M.E., Moore, C., 2004. Finding community structure in very large networks. Phys Rev E Stat Nonlin Soft Matter Phys 70**,** 066111.

Danon, L., Diaz-Guilera, A., Duch, J., Arenas, A., 2005. Comparing community structure identification. J. Stat. Mech.**,** P09008.

Dehaene, S., Kerszberg, M., Changeux, J.-P., 1998. A neuronal model of a global workspace in effortful cognitive tasks. Proc. Natl. Acad. Sci. USA 95**,** 14529-14534.

Dodel, S., Golestani, N., Pallier, C., Elkouby, V., Le Bihan, D., Poline, J.B., 2005. Condition-dependent functional connectivity: syntax networks in bilinguals. Philos. Trans. R. Soc. Lond. B Biol. Sci. 360**,** 921-935.

Duvernoy, H.M., Bourgouin, P., 1999. The human brain : surface, three-dimensional sectional anatomy with MRI, and blood supply, Springer, Wien; New York.

Eisenberger, N.I., Lieberman, M.D., Satpute, A.B., 2005. Personality from a controlled processing perspective: an fMRI study of neuroticism, extraversion, and self-consciousness. Cogn. Affect. Behav. Neurosci. 5**,** 169-181.

Engen, T., Ross, B.M., 1973. Long-term memory of odors with and without verbal descriptions. J. Exp. Psychol. 100**,** 221-227.

Eysenck, H., 1967. The Biological Basis of Personality, Thomas, Springfield, IL.

Fair, D.A., Cohen, A.L., Power, J.D., Dosenbach, N.U., Church, J.A., Miezin, F.M., Schlaggar, B.L., Petersen, S.E., 2009. Functional brain networks develop from a "local to distributed" organization. PLoS Comput. Biol. 5**,** e1000381.

Fornito, A., Zalesky, A., Breakspear, M., 2013. Graph analysis of the human connectome: Promise, progress, and pitfalls. Neuroimage 80**,** 426-444.

Fortunato, S., Barthelemy, M., 2007. Resolution limit in community detection. Proc Natl Acad Sci U S A 104**,** 36-41.

Fortunato, S., 2010. Community detection in graphs. Physics Reports 486**,** 75-174.

Fox, M.D., Snyder, A.Z., Vincent, J.L., Corbetta, M., Van Essen, D.C., Raichle, M.E., 2005. The human brain is intrinsically organized into dynamic, anticorrelated functional networks. Proc. Natl. Acad. Sci. USA 102**,** 9673-9678.

Friston, K.J., 1994. Functional and effective connectivity in neuroimaging: A synthesis. Hum. Brain Mapp. 2**,** 56-78.

Friston, K.J., Ashburner, J., Frith, C., Poline, J.B., Healther, J.D., Frackowiak, R.S., 1995. Spatial Registration and Normalization of Images. Hum. Brain Mapp. 2**,** 165-189.

Friston, K.J., Buechel, C., Fink, G.R., Morris, J., Rolls, E., Dolan, R.J., 1997. Psychophysiological and modulatory interactions in neuroimaging. Neuroimage 6**,** 218-229.

Friston, K.J., Fletcher, P., Josephs, O., Holmes, A., Rugg, M.D., Turner, R., 1998. Event-Related fMRI: Characterizing Differential Responses. NeuroImage 7**,** 30-40.

Friston, K.J., Harrison, L., Penny, W., 2003. Dynamic causal modelling. Neuroimage 19**,** 1273-1302.

Gao, Q., Xu, Q., Duan, X., Liao, W., Ding, J., Zhang, Z., Li, Y., Lu, G., Chen, H., 2013. Extraversion and neuroticism relate to topological properties of resting-state brain networks. Front. Hum. Neurosci. 7**,** 257.

Ginestet, C., Simmons, A., 2011. Statistical parametric network analysis of functional connectivity dynamics during a working memory task. Neuroimage 55**,** 688-704.

Gómez, S., Jensen, P., Arenas, A., 2009. Analysis of community structure in networks of correlated data. Phys. Rev. E 80**,** 016114.

Good, B.H., de Montjoye, Y.A., Clauset, A., 2010. Performance of modularity maximization in practical contexts. Phys Rev E Stat Nonlin Soft Matter Phys 81**,** 046106.

Good, P.I., 1994. Permutation tests : a practical guide to resampling methods for testing hypotheses, Springer-Verlag, New York.

Gottfried, J.A., Zald, D.H., 2005. On the scent of human olfactory orbitofrontal cortex: meta-analysis and comparison to non-human primates. Brain Res. Rev. 50**,** 287-304.

Guimerà, R., Sales-Pardo, M., Amaral, L.A.N., 2004. Modularity from fluctuations in random graphs and complex networks. Phys. Rev. E 70**,** 025101.

Guitart-Masip, M., Barnes, G.R., Horner, A., Bauer, M., Dolan, R.J., Duzel, E., 2013. Synchronization of medial temporal lobe and prefrontal rhythms in human decision making. J. Neurosci. 33**,** 442-451.

Haase, L., Wang, M., Green, E., Murphy, C., 2011. Functional connectivity during recognition memory in individuals genetically at risk for Alzheimer's disease. Hum. Brain Mapp. 34**,** 530-542.

Harkins, S., Geen, R.G., 1975. Discriminability and criterion differences bet<een extraverts and introverts during vigilance. J. Res. Personality 9**,** 335-340.

He, Y., Wang, J., Wang, L., Chen, Z.J., Yan, C., Yang, H., Tang, H., Zhu, C., Gong, Q., Zang, Y., Evans, A.C., 2009. Uncovering intrinsic modular organization of spontaneous brain activity in humans. PLoS One 4**,** e5226.

Hopfinger, J.B., Büchel, C., Holmes, A.P., Friston, K.J., 2000. A Study of Analysis Parameters That Influence the Sensitivity of Event-Related fMRI Analyses. NeuroImage 11**,** 326-333.

Horwitz, B., 2003. The elusive concept of brain connectivity. Neuroimage 19**,** 466-470.

Karunanayaka, P., Eslinger, P.J., Wang, J.L., Weitekamp, C.W., Molitoris, S., Gates, K.M., Molenaar, P.C., Yang, Q.X., 2013. Networks involved in olfaction and their dynamics using independent component analysis and unified structural equation modeling. Hum. Brain Mapp.**,** 10.1002/hbm.22312.

Kashtan, N., Alon, U., 2005. Spontaneous evolution of modularity and network motifs. Proc. Natl. Acad. Sci. USA 102**,** 13773-13778.

Kayser, A.S., Buchsbaum, B.R., Erickson, D.T., D'Esposito, M., 2010. The functional anatomy of a perceptual decision in the human brain. J. Neurophysiol. 103**,** 1179-1194.

Kelly, A.M., Uddin, L.Q., Biswal, B.B., Castellanos, F.X., Milham, M.P., 2008. Competition between functional brain networks mediates behavioral variability. Neuroimage 39**,** 527-37.

Kim, H., Cabeza, R., 2009. Common and specific brain regions in high- versus low-confidence recognition memory. Brain Res. 1282**,** 103-113.

Kim, H., 2013. Differential neural activity in the recognition of old versus new events: an activation likelihood estimation meta-analysis. Hum. Brain Mapp. 34**,** 814-836.

Kim, S.H., Hwang, J.H., Park, H.S., Kim, S.E., 2008. Resting brain metabolic correlates of neuroticism and extraversion in young men. Neuroreport 19**,** 883-886.

Kirwan, C.B., Stark, C.E., 2004. Medial temporal lobe activation during encoding and retrieval of novel face-name pairs. Hippocampus 14**,** 919-930.

Krusemark, E.A., Li, W., 2012. Enhanced Olfactory Sensory Perception of Threat in Anxiety: An Event-Related fMRI Study. Chemosens. Percept. 5**,** 37-45.

Langer, N., Pedroni, A., Jäncke, L., 2013. The Problem of Thresholding in Small-World Network Analysis. PLoS One 8**,** e53199.

Liu, X., Hairston, J., Schrier, M., Fan, J., 2011. Common and distinct networks underlying reward valence and processing stages: a meta-analysis of functional neuroimaging studies. Neurosci. Biobehav. Rev. 35**,** 1219-12136.

Lockhart, R.S., Murdock, B.B., 1970. Memory and the theory of signal detection. Psychol. Bull. 74**,** 100-109.

Mai, J.K., Paxinos, G., Voss, T., 2008. Atlas of the human brain, Elsevier Acad. Press, Amsterdam usw.

Manly, B.F.J., 1998. Randomization, Bootstrap and Monte Carlo Methods in Biology, Chapman & Hall.

Matsumoto, K., Suzuki, W., Tanaka, K., 2003. Neuronal correlates of goal-based motor selection in the prefrontal cortex. Science 301**,** 229-232.

Matthews, G., Gilliland, K., 1999. The personality theories of H.J. Eyseck abd J.A. Gray: a comparative review. Pers. Indiv. Diff. 26**,** 583-626.

McKeown, M.J., Sejnowski, T.J., 1998. Independent component analysis of fMRI data: examining the assumptions. Hum. Brain Mapp. 6**,** 368-372.

Mclntosh, A., Gonzalez-Lima, F., 1994. Structural equation modeling and its application to network analysis in functional brain imaging. Hum. Brain Mapp. 2**,** 2-22.

Mesulam, M.M., 1990. Large-scale neurocognitive networks and distributed processing for attention, language, and memory. Ann. Neurol. 28**,** 597-613.

Meunier, D., Achard, S., Morcom, A., Bullmore, E., 2009a. Age-related changes in modular organization of human brain functional networks. Neuroimage 44**,** 715-723.

Meunier, D., Lambiotte, R., Fornito, A., Ersche, K.D., Bullmore, E.T., 2009b. Hierarchical modularity in human brain functional networks. Front. Neuroinform. 3**,** 37.

Meunier, D., Lambiotte, R., Bullmore, E.T., 2010. Modular and hierarchically modular organization of brain networks. Front. Neurosci. 4.

Moritz, S., Glascher, J., Sommer, T., Buchel, C., Braus, D.F., 2006. Neural correlates of memory confidence. Neuroimage 33**,** 1188-1193.

Moussa, M.N., Steen, M.R., Laurienti, P.J., Hayasaka, S., 2012. Consistency of network modules in resting-state FMRI connectome data. PLoS One 7**,** e44428.

Newman, M.E.J., 2004. Analysis of weighted networks. Phys. Rev. E. 70**,** 056131.

Newman, M.E.J., Girvan, M., 2004. Finding and evaluating community structure in networks. Physical Review E 69**,** 026113.

Newman, M.E.J., Barabási, A.-L., Watts, D.J., 2006. The structure and dynamics of networks, Princeton University Press, Princeton, N.J.; Oxford.

Nigri, A., Ferraro, S., D'Incerti, L., Critchley, H.D., Bruzzone, M.G., Minati, L., 2013. Connectivity of the amygdala, piriform, and orbitofrontal cortex during olfactory stimulation: a functional MRI study. NeuroReport 24**,** 171-175.

Park, C.-H., Boudrias, M.-H., Rossiter, H., Ward, N.S., 2012. Age-related changes in the topological architecture of the brain during hand grip. Neurobiol. Aging 33**,** 833.e27-833.e27.

Penny, W.D., Stephan, K.E., Mechelli, A., Friston, K.J., 2004. Modelling functional integration: a

comparison of structural equation and dynamic causal models. Neuroimage 23 Suppl 1**,** S264-274.

Plailly, J., Howard, J.D., Gitelman, D.R., Gottfried, J.A., 2008. Attention to odor modulates thalamocortical connectivity in the human brain. J. Neurosci. 28**,** 5257-5267.

Power, J.D., Barnes, K.A., Snyder, A.Z., Schlaggar, B.L., Petersen, S.E., 2012. Spurious but systematic correlations in functional connectivity MRI networks arise from subject motion. Neuroimage 59**,** 2142-2154.

Rauch, S.L., Milad, M.R., Orr, S.P., Quinn, B.T., Fischl, B., Pitman, R.K., 2005. Orbitofrontal thickness, retention of fear extinction, and extraversion. Neuroreport 16**,** 1909-1912.

Reichardt, J., Bornholdt, S., 2006. Statistical mechanics of community detection. Phys Rev E Stat Nonlin Soft Matter Phys 74**,** 016110.

Rissman, J., Gazzaley, A., D'Esposito, M., 2004. Measuring functional connectivity during distinct stages of a cognitive task. Neuroimage 23**,** 752-763.

Roebroeck, A., Formisano, E., Goebel, R., 2011. The identification of interacting networks in the brain using fMRI: Model selection, causality and deconvolution. Neuroimage 58**,** 296-302.

Rogers, B.P., Morgan, V.L., Newton, A.T., Gore, J.C., 2007. Assessing functional connectivity in the human brain by fMRI. Magn. Reson. Imaging 25**,** 1347-1357.

Rose, C.L., Murphy, L.B., Byard, L., Nikzad, K., 2002. The role of the big five personality factors in vigilance performance and workload. Eur. J. Personality 16**,** 185-200.

Royet, J.P., Koenig, O., Gregoire, M.C., Cinotti, L., Lavenne, F., Le Bars, D., Costes, N., Vigouroux, M., Farget, V., Sicard, G., Holley, A., Mauguiere, F., Comar, D., Froment, J.C., 1999. Functional anatomy of perceptual and semantic processing for odors. J. Cogn. Neurosci. 11**,** 94-109.

Royet, J.P., Hudry, J., Zald, D.H., Godinot, D., Gregoire, M.C., Lavenne, F., Costes, N., Holley, A., 2001. Functional neuroanatomy of different olfactory judgments. Neuroimage 13**,** 506-519.

Royet, J.P., Morin-Audebrand, L., Cerf-Ducastel, B., Haase, L., Issanchou, S., Murphy, C., Fonlupt, P., Sulmont-Rosse, C., Plailly, J., 2011. True and false recognition memories of odors induce distinct neural signatures. Front. Hum. Neurosci. 5**,** 65.

Rubinov, M., Sporns, O., 2011. Weight-conserving characterization of complex functional brain networks. NeuroImage 56**,** 2068-2079.

Rushworth, M.F., Walton, M.E., Kennerley, S.W., Bannerman, D.M., 2004. Action sets and decisions in the medial frontal cortex. Trends Cogn. Sci. 8**,** 410-417.

Sales-Pardo, M., Guimerà, R., Moreira, A.A., Amaral, L.A.N., 2007. Extracting the hierarchical organization of complex systems. Proc. Natl. Acad. Sci. USA 104**,** 15224-15229.

Savic, I., Gulyas, B., Larsson, M., Roland, P., 2000. Olfactory functions are mediated by parallel

and hierarchical processing. Neuron 26**,** 735-745.

Shanahan, M., 2010. Metastable chimera states in community-structured oscillator networks. Chaos 20**,** 013108.

Shidara, M., Richmond, B.J., 2002. Anterior cingulate: single neuronal signals related to degree of reward expectancy. Science 296**,** 1709-1711.

Shinkareva, S.V., Mason, R.A., Malave, V.L., Wang, W., Mitchell, T.M., Just, M.A., 2008. Using FMRI brain activation to identify cognitive states associated with perception of tools and dwellings. PLoS One 3**,** e1394.

Simon, H.A., 1962. The architecture of complexity. Proc. Am. Phil. Soc. 106**,** 467-482.

Snodgrass, J.G.C., J., 1988. Pragmatics of measuring recognition memory: applications to dementia and amnesia. J. Exp. Psychol. Gen. 117**,** 34-50.

Spors, H., Albeanu, D.F., Murthy, V.N., Rinberg, D., Uchida, N., Wachowiak, M., Friedrich, R.W., 2012. Illuminating vertebrate olfactory processing. J. Neurosci. 32**,** 14102-14108.

Stark, C.E., Squire, L.R., 2000. Functional magnetic resonance imaging (fMRI) activity in the hippocampal region during recognition memory. J. Neurosci. 20**,** 7776-7781.

Stevens, A.A., Tappon, S.C., Garg, A., Fair, D.A., 2012. Functional brain network modularity captures inter- and intra-individual variation in working memory capacity. PLoS One 7**,** e30468.

Ter Braak, C.J.F., 1992. Permutation versus bootstrap significance tests in multiple regression and ANOVA. In: Bootstrapping and related techniques. K.H. Jöckel, G. Rothe, W. Sendler, ed. Springer-Verlag, Berlin, Heidelberg, pp. 79-86.

Traag, V.A., Bruggeman, J., 2009. Community detection in networks with positive and negative links. Phys. Rev. E 80**,** 036115.

Varela, F., Lachaux, J.P., Rodriguez, E., Martinerie, J., 2001. The brainweb: phase synchronization and large-scale integration. Nat. Rev. Neurosci. 2**,** 229-239.

Vigouroux, M., Bertrand, B., Farget, V., Plailly, J., Royet, J.P., 2005. A stimulation method using odors suitable for PET and fMRI studies with recording of physiological and behavioral signals. J. Neurosci. Meth. 142**,** 35-44.

Wang, L., Li, Y., Metzak, P., He, Y., Woodward, T.S., 2010. Age-related changes in topological patterns of large-scale brain functional networks during memory encoding and recognition. Neuroimage 50**,** 862-872.

Ward, J.H., 1963. Hierarchical grouping to optimize an objective function. J. Am. Statis. Assoc. 58**,** 236-244.

Wilson, D.A., Yan, X., 2010. Sleep-like states modulate functional connectivity in the rat olfactory system. J. Neurophysiol. 104**,** 3231-3239.

Wilson, D.A., Hoptman, M.J., Gerum, S.V., Guilfoyle, D.N., 2011. State-dependent functional

connectivity of rat olfactory system assessed by fMRI. Neurosci. Lett. 497**,** 69-73.

Zald, D.H., Donndelinger, M.J., Pardo, J.V., 1998. Elucidating dynamic brain interactions with across-subjects correlational analyses of positron emission tomographic data: the functional connectivity of the amygdala and orbitofrontal cortex during olfactory tasks. J. Cereb. Blood Flow Metab. 18**,** 896-905.

Zelano, C., Bensafi, M., Porter, J., Mainland, J., Johnson, B., Bremner, E., Telles, C., Khan, R., Sobel, N., 2005. Attentional modulation in human primary olfactory cortex. Nat. Neurosci. 8**,** 114-120.